



# Springback analysis of different A-values of Cu and Al tubes in free bending forming technology: experimentation and finite element modeling

Wei Wang<sup>1</sup> · Shenghan Hu<sup>1,2</sup> · Ali Abd El-Aty<sup>1,2,3</sup> · Cong Wu<sup>1,2</sup> · Qiucheng Yang<sup>1,2</sup> · Hao Chen<sup>1,2</sup> · Yizhou Shen<sup>1</sup> · Jie Tao<sup>1,2</sup>

Received: 16 June 2020 / Accepted: 7 December 2020 / Published online: 26 January 2021  
© The Author(s), under exclusive licence to Springer-Verlag London Ltd. part of Springer Nature 2021

## Abstract

In tube free bending forming technology, the springback behavior affects the bent tubes' forming accuracy and quality. Thus, in this investigation, the springback behaviors of T2-Cu and AA6061-T6 tubes manufactured by free bending technology were studied experimentally and using finite element modeling. The bending radius of the formed tubes was measured in ABAQUS combined with the geometric calculation. After investigating the different A-values (sufficient length of deformation zone) of Cu and Al tubes, it was found that the higher the A-value, the higher the bending angle, the lower the bending radius, and the larger the springback angle. The changes of both bending and material properties affect the springback to specific values. The tube forming's stress peak occurred in the forming segment, where the springback angle is the highest, and the outer springback is higher than the inner side at the same A-value and position. Under the same forming parameters, each section's strain variation and springback angle in the bending process of T2-Cu tubes is higher than that of AA6061-T6 tubes. The simulation results were in remarkable agreement with those obtained from experimentation, proving the simulation's reliability and accuracy.

**Keywords** 3D free bending · Springback · T2-Cu · AA6061-T6 · A-value · Forming section

## 1 Introduction

The bending components manufactured from different metallic materials have a wide range of applications in many fields, such as aerospace, aircraft, and automotive industries [1]. Some different small bending radius pipes also play an essential role in the piping system of various engineering fields [2]. Three-dimensional free bending forming technology is a novel tube vector forming technology. Meanwhile, free-forming of different thin-walled complex-shaped components and

small bending radii can easily achieve great significance for modern tube processing [3].

Under the same process parameters, tube specifications, and equipment conditions while forming the tubes using a free bending process, the formed tubes often possess different bending radii and bending angles. This is usually caused by the differences in the mechanical properties of the tube materials. The key reason is that there is still some elastic stress during the free bending tubes' plastic deformation. After completing the forming process, the change in shape caused by the decrease of stress in the formed tubes creates the bending angle and bending radius to fail to reach the target angle [4]. The existence of tube springback usually affects the accuracy and quality of the formed component [5]. Therefore, it is significant to investigate the springback behavior of different materials in the free bending forming technology to obtain accurate and high-quality tubes.

Daxin et al. [6] proposed a novel theoretical analysis model, which took into account the strain hardening of the tube to analyze the time-dependent springback behavior. They also combined the finite element simulation to study the stress distribution in the bending process and calculated the amount

✉ Jie Tao  
taojie@nuaa.edu.cn

<sup>1</sup> College of Material Science and Technology, Nanjing University of Aeronautics and Astronautics, Nanjing 211100, People's Republic of China

<sup>2</sup> Jiangsu Key Laboratory of Nuclear Energy Equipment Materials Engineering, Nanjing University of Aeronautics and Astronautics, Nanjing 211100, People's Republic of China

<sup>3</sup> Mechanical Engineering Department, Faculty of Engineering-Helwan, Helwan University, Cairo, Egypt

of springback. Zhan et al. [7] clarified the springback mechanism during the NC bending process. They analyzed the relative bending radius, strengthening factor, and material hardening coefficient on the springback angle. Cai et al. [8] established a model for predicting the springback angle of components with large curvature and studied the influence of relevant process parameters such as bending angle and bending speed on the tubes' springback. Zhu et al. [9] compared the effects of the process conditions on the springback and section deformation. They revealed the coupling effect of the springback and section deformation during the bending process. Furthermore, they established a theoretical model to predict the springback angle and investigated how to control springback under different filling conditions through this model. Liao et al. [10] studied the springback and twisting deformation of aluminum alloy tubes during NC bending. Besides, they studied the tube's stress distributions at different forming stages and revealed its effect on the springback mechanism. Wang et al. [11] conducted experiments to investigate process parameters' influence on section deformation and springback of thin-walled CNC bending tubes. Zhai et al. [12] examined the springback of profiles with arbitrary cross-section shapes under different loading methods. They predicted the deformation modes and springback of rectangular tubes and U-shaped tubes. This leads to providing theoretical models for the flexible manufacturing of the whole process profiles and intelligent control. Wu et al. [13] extended the calculation method to the loading modes considering the strain strengthening recovery. They investigated the springback mechanism of the space bent tubes and the influence of the loading modes. Zhou et al. [14] explore the impacts of the residual stress and springback on the forming quality and geometric accuracy of SS304 bent tubes. Kwang-Hyun Ahn et al. [15] proposed a feasible springback prediction method, which combined with the existing theory to predict the critical final dimensions of the complex members in the curved space. It can be used for efficient initial layout and space design of the spiral tube steam generators. Gu et al. [16] studied the springback behavior of thin-walled tubes in NC bending and combined dynamic explicit and the static implicit algorithm to calculate the whole process of thin-walled tube NC precision bending. Li et al. [17] investigated process parameters (e.g., friction, clearance, and mobile die section shape) on bending springback after the free bending process. They discussed the impact of process parameters on the final springback of the pipe.

Based on the aforementioned discussion, it is clear that the impact of the springback of profiles with different materials on the final bending radius, bending angle, and stresses of the tube during different free bending forming stages is not investigated. Thus, in this investigation, the springback behavior's impact on the bending radius and bending angle of T2-Cu and AA6061-T6 free bending tubes was analyzed theoretically

and by FE simulation. According to the initial A-value of the free bending forming equipment, the FE simulations and actual forming experiments were carried out. The differences between the forming bending radius and angle, and the calculating radius and angle were discussed. By increasing the A-value gradually, the springback corrections were performed on the tubes with different materials. Besides, the stresses change laws of the tube during and at the forming process were explored.

## 2 Theoretical analysis

### 2.1 Bending moment of the 3D flexible bending

The main technical principle of three-axis three-dimensional free bending is depicted in Fig. 1. The billet is pushed from the guide rail to the bending die by the axial force  $P_L$ , and the bending occurs accordingly. The distance between the center axis of the guide and the center axis of the bending die is called eccentricity  $U$ . The distance between the center of the die and the exit of the guide rail is called  $A$ , and  $A$  does not change during the bending process. The complex geometry was formed through continuously adjusting the location of the bend die via the control of X- and Y-directions servo motors. Meantime, the friction force  $f$  between the billet and the bending die can be divided into  $f_x$  in X-direction and  $f_y$  in Y-direction. The bending moment  $M$  is expressed as [18]:

$$M = (P_u + f_y) * A + (P_L + f_x) * U \quad (1)$$

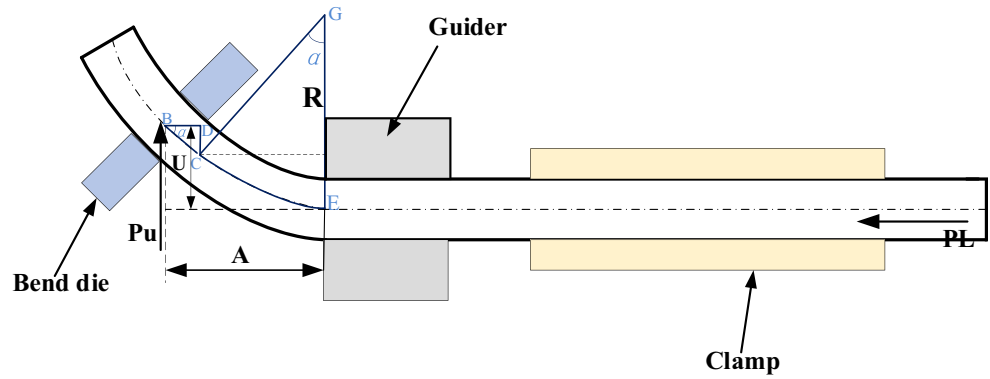
### 2.2 Process analysis of 3D flexible bending forming

The tube's final geometry is determined by the movement locus of the bend die during the 3D free bending. Generally, the bending process of the tubes was divided into three sections, as presented in Fig. 2. The transition occurred at the beginning and the end of the tube bending, called Section 1 (L1) and Section 3 (L3). Section 2 (L2) referred to the arc section. The bend die moved through the spherical bearing from the balance position to a position with  $U_{max}$ 's eccentricity in Section 1. Then, the bend die stops moving and keeps in the maximal position in Section 2. Meanwhile, the tube is kept being pushed until reaching the desired bending angle. In Section 3, the bend die moves similar to L1. The bend die was returned to its original position, and the eccentricity is reduced to 0 [19].

### 2.3 Calculation method of bending radius

As shown in Fig. 1, when the bending die starts to move towards the position with an eccentricity of  $U$ , the bending

**Fig. 1** The schematic description of the principle of the 3D free bending process



die and the guider show a state of a combination of straight segment and arc segment, that is,  $BC + \widehat{CE}$ . After the bending die reaches the target position, all the curves between the bending die and the guide are arc segments. The transition segment and the transition segment get the maximum value.

So,  $U$  can be described as the following equation:

$$U = DC + FE = DC + (R - R \cdot \cos \alpha) \tag{2}$$

This equation can also be derived from Fig. 1:

$$A = BD + CF = BD + R \cdot \sin \alpha \tag{3}$$

Combining Eqs. (2) and (3) and the geometric relationship in Fig. 1, thus  $U$ - $R$  relationship can be rewritten as:

$$U = R - \sqrt{R^2 - A^2} \tag{4}$$

At this time, ensure that  $R$  is unchanged, give  $A$  value a scaling factor  $k$ , and get the value of eccentricity  $U'$  when  $A$  value is  $kA$ :

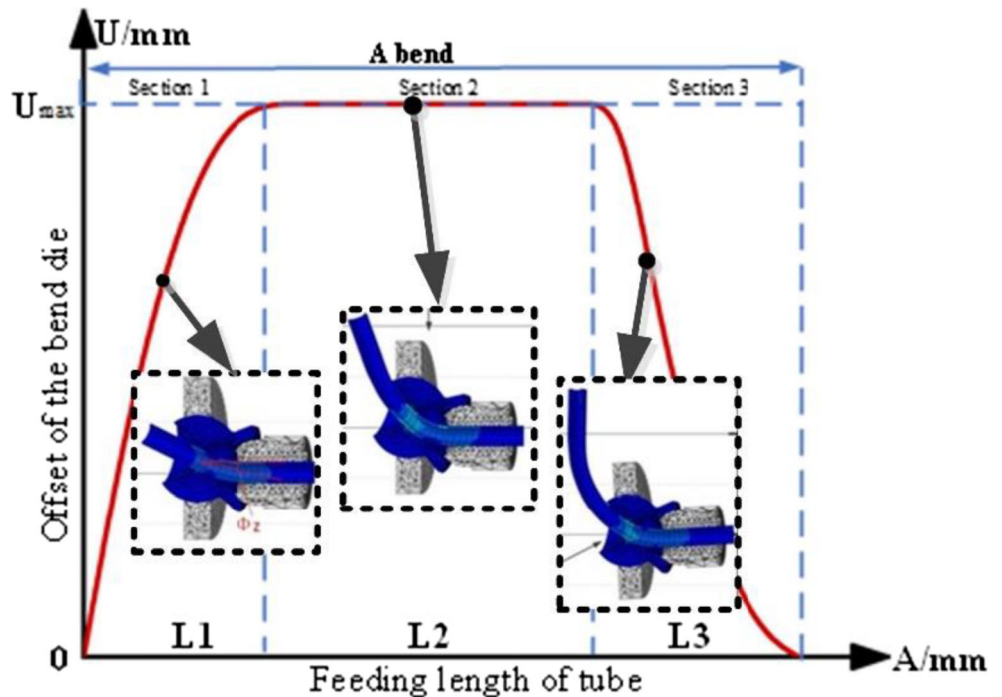
$$U' = (kA - R \cdot \sin \alpha) \cdot \tan \alpha + (R - R \cdot \cos \alpha) \tag{5}$$

Then, substituting the  $U'$  calculated from Eq. (5) into Eq. (4) inversely solves the bending radius  $R'$  at this time:

$$R' = \frac{1}{2} \cdot \left( U' + \frac{A^2}{U'} \right) \tag{6}$$

Through the experiments, the eccentricity  $U$  of the actual bending process of the tube can be measured. Combining with the different  $kA$  values set by us, Eq. (6) can be used to solve the bending radius  $R'$  of the tube inversely. After that, the measured  $R$  and  $\theta$  value in the finite element simulation was

**Fig. 2** Schematic diagram of tube free bending process



compared with the experimental calculation result. The following relationship is obtained:

$$\begin{cases} \Delta R = R - R' \\ \Delta \theta = \frac{180vt}{\pi R} - \frac{180vt}{\pi R'} \end{cases} \quad (7)$$

where  $v$  is the tube's feeding speed, and  $t$  is the total time of the forming process.

## 2.4 Springback analysis of 3D flexible bending

The 3D free bending forming process is similar to other deformation processes, where it can be composed of elastic and plastic deformation under the action of external load. After unloading, the plastic deformation of the tube remains while the elastic deformation recovers. The material layer on the outside of the bending neutral layer shortens due to the elastic recovery and the inside stretches the layer. Therefore, the tube changes bending radius and angle change after forming called springback [20].

Because free bending belongs to flexible forming under less restrictive conditions, the tube is in an unconstrained state after exiting from the bending die's front end. At this time, partial springback of the formed tube has occurred. Therefore, the tube's total springback after free bending is formed by the cumulative springback of several parts during the forming process. Simultaneously, considering the particularity of the analytical algorithm for the free bending transition section, the transition section's dimensional error, which is a combination of straight and curved sections, is also included in the springback of free bending.

According to the stress-strain relationship, for the thin-walled tube, the radial compressive stress between the layer can be ignored so that the stress-strain relationship can be described as following [21]:

$$\begin{cases} \varepsilon_\theta = \frac{\bar{\varepsilon}}{\bar{\sigma}} \left( \sigma_\theta - \frac{1}{2} \sigma_D \right) \\ \varepsilon_D = \frac{\bar{\varepsilon}}{\bar{\sigma}} \left( \sigma_D - \frac{1}{2} \sigma_\theta \right) \end{cases} \quad (8)$$

where  $\sigma_\theta$  and  $\sigma_D$  represent tangential and circumferential stress, respectively. And  $\varepsilon_\theta$  and  $\varepsilon_D$  represent tangential and circumferential strain. For simplicity, it is assumed that the material does not produce circumferential flow during the bending process, so the circumferential strain of the tube is  $\varepsilon_D = 0$ . Thus, and the strain state of the material is considered a plane strain state. Therefore, Eq. (9) is expressed as:

$$\sigma_D = \frac{1}{2} \sigma_\theta \quad (9)$$

Therefore, the equivalent stress was introduced by Eq. (10):

$$\bar{\sigma} = \sqrt{\sigma_\theta^2 + \sigma_D^2 - \sigma_\theta \sigma_D} = \sqrt{\sigma_\theta^2 + \left( \frac{1}{2} \sigma_\theta \right)^2 - \sigma_\theta \cdot \frac{1}{2} \sigma_\theta} = \frac{\sqrt{3}}{2} \sigma_\theta \quad (10)$$

Because of the particularity of free bending, considering the tangential compressive stress ( $\sigma_N$ ) caused by the axial thrust, the equation of the equivalent stress can be derived as following [22]:

$$\bar{\sigma} = \frac{\sqrt{3}}{2} \sigma_\theta + \sigma_N \quad (11)$$

According to the incompressible condition of the plastic deformation material:

$$\varepsilon_\theta + \varepsilon_D + \varepsilon_t = 0 \quad (12)$$

Then, substitute Eqs. (9) and (11) into the Eq. (8), and the equivalent strain was obtained as:

$$\bar{\varepsilon} = \frac{4}{3} \varepsilon_\theta \cdot \frac{\bar{\sigma}}{\sigma_\theta} = \frac{2}{\sqrt{3}} \varepsilon_\theta \left( 1 + \frac{2\sigma_N}{\sqrt{3}\sigma_\theta} \right) \quad (13)$$

As demonstrated in Fig. 3, Eq. (13) can also be described as:

$$\bar{\varepsilon} = \frac{2}{\sqrt{3}} \varepsilon_\theta \left( 1 + \frac{2\sigma_N}{\sqrt{3}\sigma_\theta} \right) = \frac{2R_m \cdot \sin\theta}{\sqrt{3}\rho} \left( 1 + \frac{2\sigma_N}{\sqrt{3}\sigma_\theta} \right) \quad (14)$$

In this equation,  $\frac{d}{2} \leq R_m \leq \frac{D}{2}$ ,  $0 \leq \theta \leq 2\pi$ , and for a thin-walled tube,  $R_m \approx \frac{D}{2}$ ;  $d$  is the outer diameter and the inner diameter of the tube, respectively, and  $\rho$  is the curvature radius of the curved neutral layer [23].

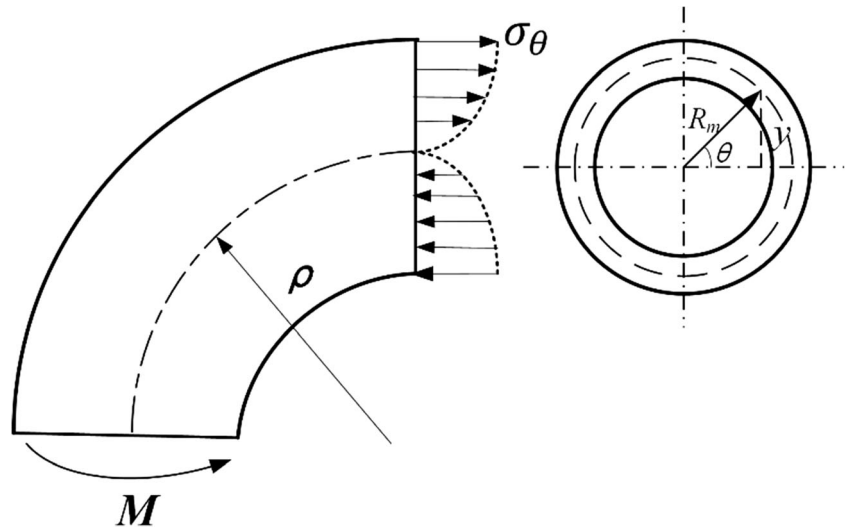
By the combination of Eqs. (11), and (14), Eq. (15) was obtained as follows:

$$\sigma_\theta = \frac{2}{\sqrt{3}} (\bar{\sigma} - \sigma_N) = \left( \frac{2}{\sqrt{3}} \right)^{n+1} \cdot B \cdot \left[ \frac{R_m \cdot \sin\theta}{\rho} \cdot \left( 1 + \frac{2\sigma_N}{\sqrt{3}\sigma_\theta} \right) \right]^n - \frac{2}{\sqrt{3}} \sigma_N \quad (15)$$

After forming, the springback of each bending section reflects the curvature radius of the bending part and the change of the bending part. As shown in Fig. 4,  $\rho$ ,  $\theta$ , and  $r$  are used to represent the radius of curvature before springback and the bending angle and the most inboard radius of curvature of the bending tube, respectively. Besides  $\rho'$ ,  $\theta'$ , and  $r'$  are used to represent the radius of curvature after springback, the bending angle, and the most inboard radius of curvature of the bending tube, respectively.

The bending radius before and after springback is composed of the incremental nominal strain before and after

Fig. 3 The distribution of stress



springback of the tube, as indicated in Eqs. (16) on the inside and (17) on the outside:

$$\theta' \cdot r' = \theta \cdot r \cdot (1 + \Delta\varepsilon_i) \tag{16}$$

$$\theta' \cdot (r' + D) = \theta \cdot (r + D) \cdot (1 + \Delta\varepsilon_o) \tag{17}$$

The assumption of the springback during the bending process is explained as follows: A and B show the increase of strain on loading as in Eq. (18) [24]:

$$\Delta\varepsilon = AY + B \tag{18}$$

where  $Y$  is the displacement of the neutral layer of the tube.

So, the springback angle  $\Delta\theta$  is written as:

$$\Delta\theta = \theta - \theta' = [-(R_m + D)A - B] \cdot \theta \tag{19}$$

It can be concluded from Eq. (15) that the springback angle  $\Delta\theta$  is related to the process parameters and the value of the bending angle. The tube's bending angle impacts the amount of springback behavior, where the higher the bending angle, the larger the deformation zone. Bending in the same condition, the unit length on the smaller deformation, the proportion of the total the deformation of the elastic deformation is increased accordingly the springback angle  $\Delta\theta$ .

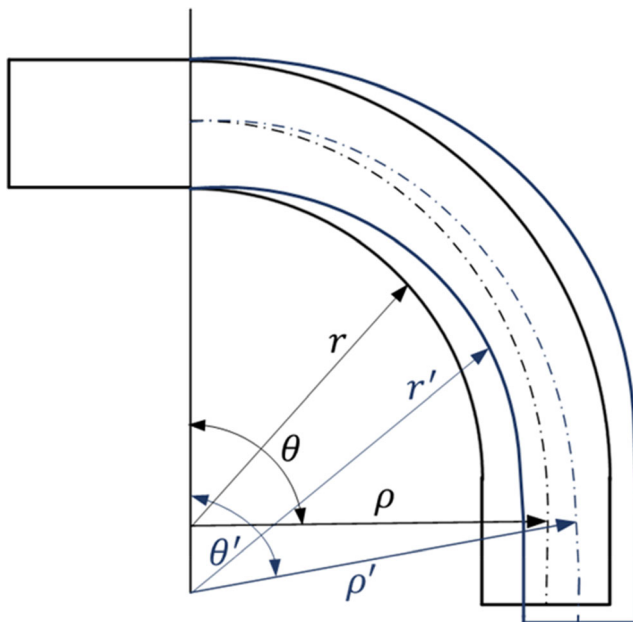


Fig. 4 Springback of bending deformation

### 3 Finite element analysis of springback during 3D free bending

#### 3.1 FE model of 3D free bending

T2-Cu tubes and AA6061-T6 tubes with the same dimensions, i.e., a diameter of 31.8 mm and a thickness of 2 mm, were used in this investigation. The density and mechanical properties of the aforementioned materials are listed in Table 1. Figure 5 depicts the finite element model, including the bending die, spherical bearing, guiding mechanism, and shaft.

Sleeve and tube were established, except the tubes are defined as deformable bodies of T2-Cu and AA6061-T6, respectively. Others are described as rigid bodies of YG8. The tube's element type is the shell element. Both aluminum and copper tubes were divided into 6250 units. The analysis step of bending simulation adopted a dynamic explicit algorithm, and the interaction was set to a general contact. The finite element

**Table 1** The density and the mechanical properties of the T2-Cu and AA6061 tubes

| Materials | Density<br>$\rho$<br>(kg/m <sup>3</sup> ) | Young's Modulus<br>$E$ (GPa) | Poisson's ratio<br>$\nu$ | Yield strength<br>$\sigma_s$ (MPa) | Tensile strength<br>$R_m$ (MPa) |
|-----------|---|------------------------------|--------------------------|------------------------------------|---------------------------------|
| T2 copper | 8.9                                       | 110                          | 0.32                     | 70                                 | 195                             |
| AA6061-T6 | 2.69                                      | 80.7                         | 0.3                      | 240                                | 260                             |

model's relevant parameters were set as follows: the clearance between tube and bending die was set to 0.05 mm, the tube axial feed speed was set to 10 mm/s, and the friction coefficient was set to 0.02.

### 3.2 Measurement of tube bending angle and radius in ABAQUS FE code

After FE simulation using Abaqus, the target parameters such as bending radius, bending angle, and the stress changes of specific points during the bending process were measured. The bending angle was measured by angle measurement function in a new simulation file in which the tubes from the simulation-completed file were imported. Due to the restriction of measuring the bending radius directly in this study, the following method, combined with the geometric calculation, was used to measure it:

- (1) Three points were picked on the formed tube and measure their coordinates using the "Query-Node" function. The unknown center coordinates and the measured three-point coordinates were marked as  $O(x_0, y_0, z_0)$ ,  $A(x_1, y_1, z_1)$ ,  $B(x_2, y_2, z_2)$ , and  $C(x_3, y_3, z_3)$ , respectively.
- (2) The following equation is the plane equation determined by  $A(x_1, y_1, z_1)$ ,  $B(x_2, y_2, z_2)$ , and  $C(x_3, y_3, z_3)$ :

$$\begin{vmatrix} x & y & z & 1 \\ x_1 & y_1 & z_1 & 1 \\ x_2 & y_2 & z_2 & 1 \\ x_3 & y_3 & z_3 & 1 \end{vmatrix} = 0 \quad (20)$$

Equation (18) can be simplified as:

$$a_1x + b_1y + c_1z + d_1 = 0 \quad (21)$$

- (3) Equations (20) and (21) can be obtained according to the geometrical condition that is equal distance from point A, B, or C to point O:

$$2(x_2 - x_1)x + 2(y_2 - y_1)y + 2(z_2 - z_1)z + x_1^2 + y_1^2 + z_1^2 - x_2^2 - y_2^2 - z_2^2 = 0 \quad (22)$$

$$2(x_3 - x_1)x + 2(y_3 - y_1)y + 2(z_3 - z_1)z + x_1^2 + y_1^2 + z_1^2 - x_3^2 - y_3^2 - z_3^2 = 0 \quad (23)$$

Equations (20, 21) can be simplified as:

$$a_2x + b_2y + c_2z + d_2 = 0 \quad (24)$$

$$a_3x + b_3y + c_3z + d_3 = 0 \quad (25)$$

**Fig. 5** The FE model of a 3D free bending system after meshing

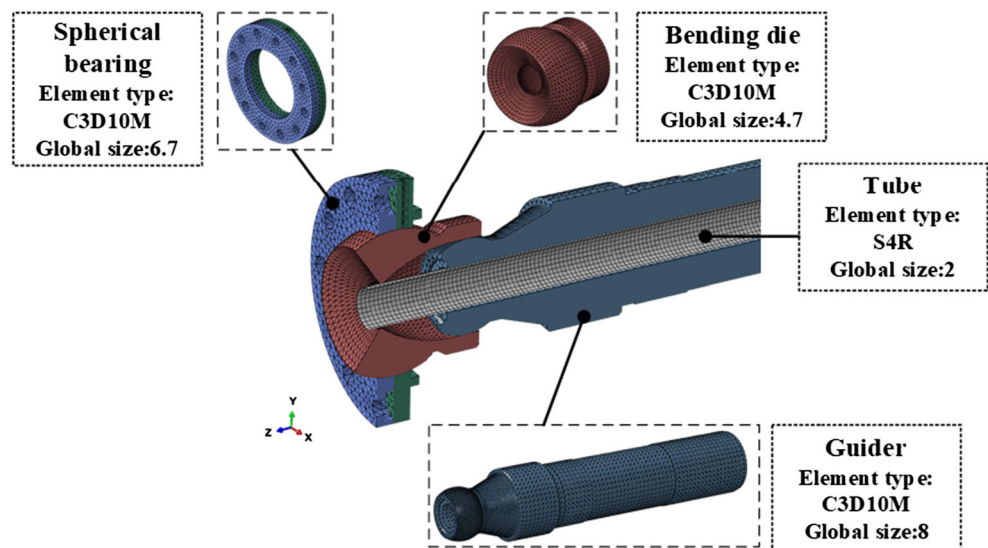
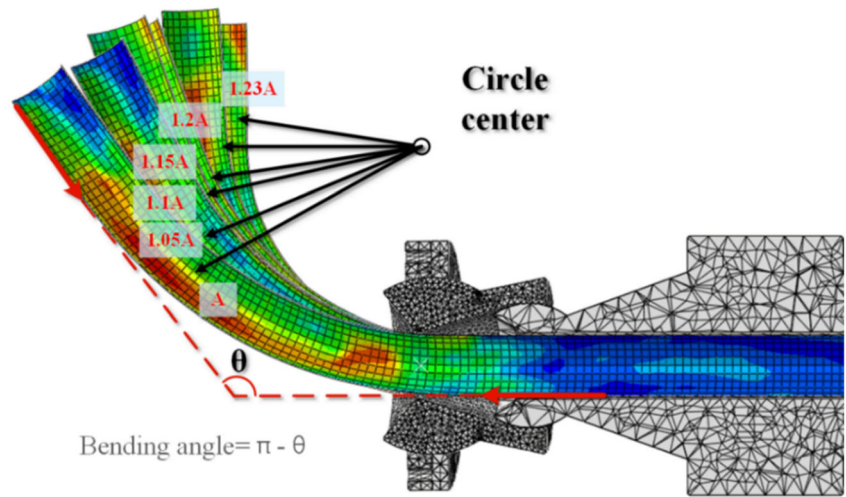


Fig. 6 Simulation results with different “A” value



(4) Combining Eqs. (19, 22, 23) leads to Eq. (24), which coordinates of point O can be solved with:

$$\begin{vmatrix} a_1 & b_1 & c_1 \\ a_2 & b_2 & c_2 \\ a_3 & b_3 & c_3 \end{vmatrix} \begin{vmatrix} x_0 \\ y_0 \\ z_0 \end{vmatrix} + \begin{vmatrix} D_1 \\ D_2 \\ D_3 \end{vmatrix} = 0 \tag{26}$$

The bending radius can be obtained with the result of Eq. (25):

$$R = \sqrt{(x_1-x_0)^2 + (y_1-y_0)^2 + (z_1-z_0)^2} \tag{27}$$

The “XY Data can obtain the Stress changes of specific points during the bending process from ODB Field Output” function.

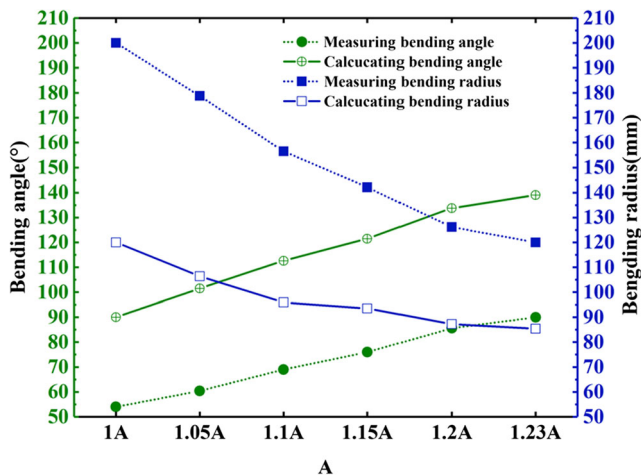


Fig. 7 Calculation value and the measurement value of bending angle, calculation value of bending radius, and change of measurement value with A

### 3.3 Analysis of the simulation results of T2-Cu tube

In the 3D bending process, “A” denotes the distance between the center point of the bending die and the front end of the guider. The original A-value in this FE model is 48. The different bending angles and the bending radius can be obtained by adjusting this parameter in theoretical calculation. During the FE simulation of T2-Cu, A was adjusted to be 1.05A, 1.1A, 1.15A, 1.2A, and 1.23A in different simulation jobs to obtain different bending angles and bending radius. The simulation results with different A-values are depicted in Fig. 6.

As depicted in Fig. 7, calculating the bending angle with the measuring bending angle and calculating the bending radius with the measuring bending radius was made. The difference between the calculating bending angle and the measuring bending angle is the springback angle. As the A-value increased, the calculating bending angle and the measuring bending angle increased

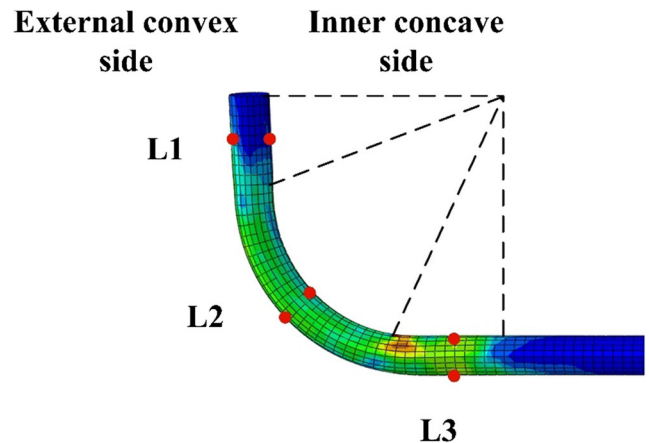
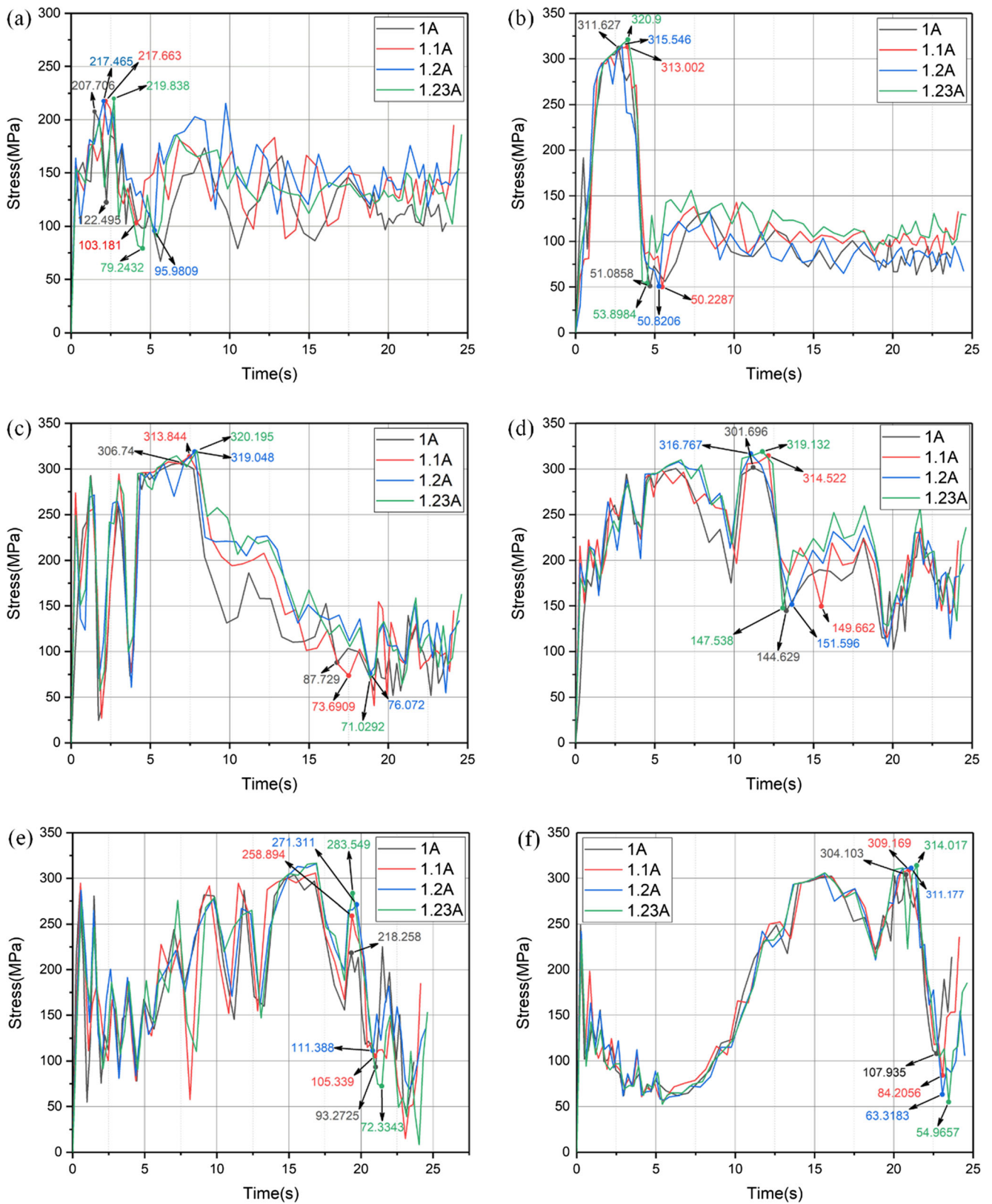


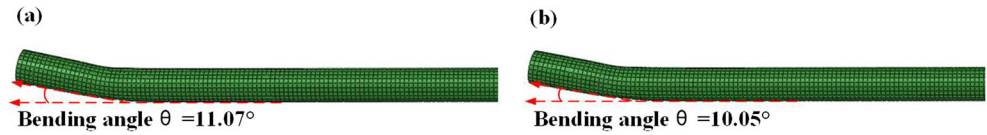
Fig. 8 Position distribution of stress measurement points



**Fig. 9** Stress changes of different sections with different “A” value. **a** Inter side of L1. **b** Outer side of L1. **c** Inter side of L2. **d** Outer side of L2. **e** Inter side of L3. **f** Outer side of L3



**Fig. 10** Comparison of bending angles of Cu tube at different times. *t* = **a** 3.28 s; **b** 3.29 s



gradually, and the difference value between them was progressively decreased. On the other hand, the calculating bending radius and the measuring bending radius decreased gradually, and the difference between them increased gradually. This is attributed to the higher bending angle. The smaller the bending radius, the higher the required external load, the more elastic deformation the tube produces during the deformation process, and the higher the springback after unloading.

To explain this law in detail, the stress measurement was selected from the formed tube’s inner and outer sides in FE simulations. As shown in Fig. 8, six stress measurement points from both inner and outer sides in L1 (the first changeover section), L2 (bending section), and L3 (the second changeover section) of each formed tube were selected. Since the tube’s springback process is a stress release process, stress changes of specific points during the bending process were obtained using the method introduced in the previous section.

As shown in Fig. 9, the maximum stress value in L1 section increased with the increase of the A-value. After the point of the maximum stress, the stress-time curve appears unstable decline, near the end of the L1 section. The “stress-time” graph line appears as the minimum mathematical value. The process from the maximum point to the minimum mathematical point is the stress release process. The value of it increased with increasing A-value both inter and outer side of formed tubes. Similar laws can be found in L2 section and L3 section, and L2 section has the largest springback, followed by L3 section and L1 section. This is attributed to the stress release in which stress accumulates over time, so as the springback. Since the bending time increases

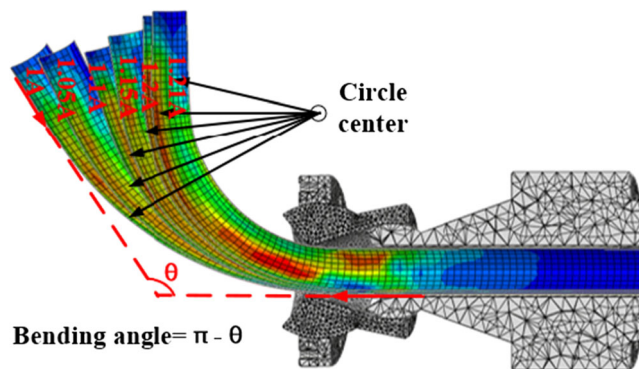


**Fig. 11** Simulation results under different A

with the increasing A-value, the bending time corresponding to the higher A-value is more extended, where the more stress accumulation, the higher the springback. It suggested that the law that the springback of tubes increases with A-value in the 3D bending process can still be drawn from the stress aspects.

It can be seen from Fig. 9b that when  $A = 1.23A$ ,  $t = 3.28$  s, the stress reaches the maximum value, and when the time increases to 4.5 s, the stress is released. It can be seen that the springback is evident in this period. However, since the bending and springback are synchronous, the simulation diagram of tube deformation shape at  $t = 3.28$  s and 3.29 s is selected for comparison, as shown in Fig. 10. It can be seen from the figure that the bending angle of the tube at  $t = 3.29$  s is slightly less than that at the time of  $t = 3.28$  s, and the bending of the tube in this short time is ignored. Therefore, it can be judged that the tube springback occurs in this short time, and the stress release process is accompanied by springback.

### 3.4 Analysis of the simulation results of AA6061 tube

#### 3.4.1 Analysis of the bending angle and bending radius

In the simulation process during deformation, A was adjusted from 1A to 1.05A, 1.1A, 1.15A 1.2A, and 1.21A. The simulation results are presented in Fig. 11.

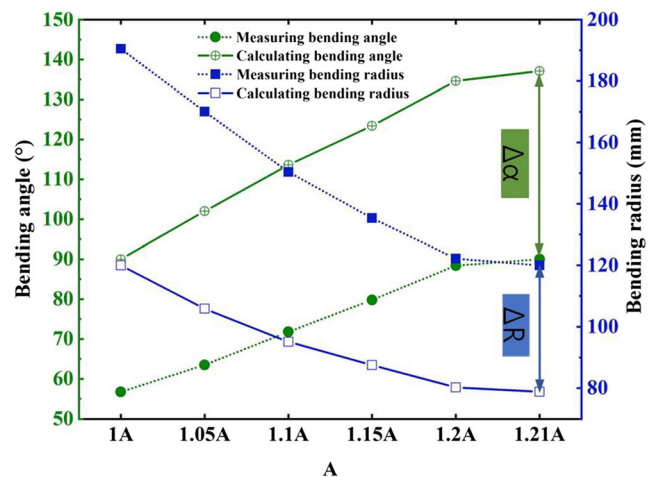


**Fig. 12** Bending angle, bending radius-A

Under different A-values, the bending radius and bending angle determined through the theoretical calculation and measurement change with A-value are depicted in Fig. 12

The change of A-value can be noticed in Fig. 12. With the increase of A-value, the bending angle obtained from the theoretical calculation and measurement has

similar trends, where, as A-value increased, the bending angle gradually increased. The bending radius obtained from the theoretical calculation and the measurement decrease with increasing the A-value.  $\Delta\alpha$  is the springback angle, which is the difference between the calculated bending angle and the measured bending

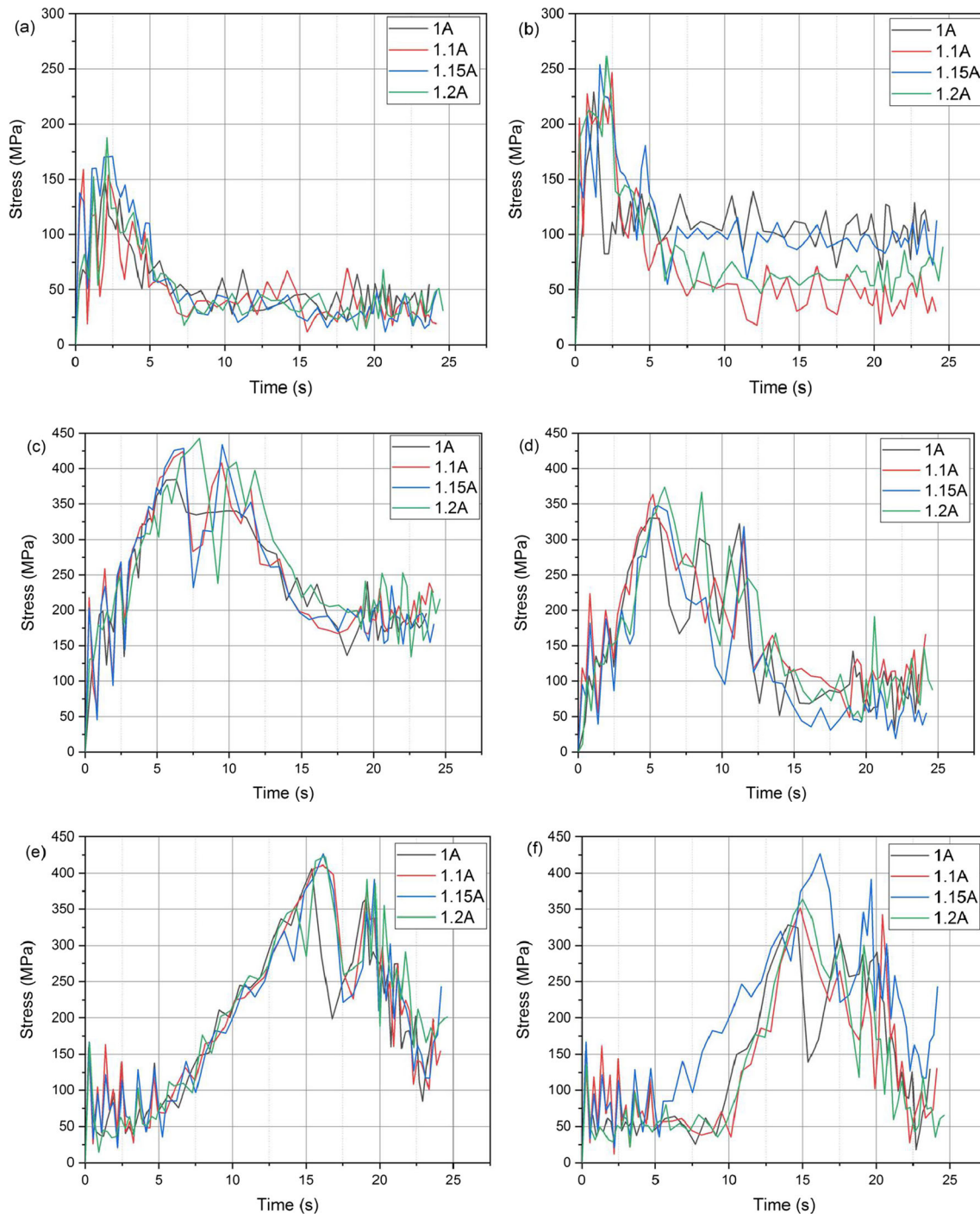


**Fig. 13** Stress-time curve of AA6061 tube at different A-values and the same position. **a** Inner side of L1. **b** Outer side of L1. **c** Inner side of L2. **d** Outer side of L2. **e** Inner side of L3. **f** Outer side of L3

**Table 2** Stress release value at different A-values and different positions

| Stress release | The inner midpoint of L1 | The outer midpoint of L1 | The inner midpoint of L2 | The outer midpoint of L2 | The inner midpoint of L3 | The outer midpoint of L3 |
|----------------|--------------------------|--------------------------|--------------------------|--------------------------|--------------------------|--------------------------|
| 1A             | 97.372                   | 146.657                  | 99.715                   | 120.54                   | 91.912                   | 141.612                  |
| 1.1A           | 94.301                   | 149.867                  | 141.304                  | 189.954                  | 124.211                  | 172.522                  |
| 1.15A          | 114.146                  | 158.876                  | 196.747                  | 205.281                  | 181.534                  | 181.534                  |
| 1.2A           | 124.224                  | 161.86                   | 204.955                  | 216.962                  | 196.884                  | 206.566                  |

angle. It is noticed from Fig. 12 that the springback angle  $\Delta\alpha$  has increased along with the augment of A-value.  $\Delta R$  decreased with increasing A-values because of increasing A, bending angle on the increase. Meanwhile, by reducing the bending radius, more materials are subject to elastic deformation, and springback is also increasing.

**3.4.2 Analysis of stress changes**

Figure 13a, b, c, d, e, and f are stress-time curves of the inner and outer sides of L1, L2, and L3, respectively. Besides, Table 2 shows the stress release value at different A-values and various positions. As shown in Fig. 13a and b and listed in Table 1, the stress peak in the whole process of tube forming occurs in the L1 segment. It increases with the increase of A. During the forming of segment L1, there was stress release. The stress release value increased with the rise in A. Besides, from Fig. 13c and d, the stress peak in the whole process of tube forming occurs in L2 segment and increases with the increase of A. When the tube is formed in the L2 section, the stress release happens. The stress release value increases with the increase of A, which is listed in Table 2. When forming the L2 segment, the stress release value is higher than forming the L1 segment, indicating that the springback at the L2 point is higher than L1.

From Fig. 13e and f, it is concluded that the peak stress in the whole process of tube forming occurs in L2 segment, and the peak stress at 1.15A is the largest. When A increases to 1.2A, the peak stress decreases again. During the forming of the L3 section, there is a stress release, and the stress release value increased with the increase of the A-value. As listed in Table 2, when

forming the L3 segment, the stress release value is between L1 and L2,  $L1 < L3 < L2$ . This is related to the forming time of L1, L2, and L3 segments. In the 3D free bending process of the Al6061 tube, L1, L2, and L3 sections all have stress release, which indicates that the springback runs through the entire tube forming process, that is, forming and springback occur simultaneously.

It can be seen from Fig. 14b that when  $A = 1.2A$ ,  $t = 2.1$  s, the stress reaches the maximum value, and when the time increases to 2.7 s, the stress is released. It can be seen that the springback is evident in this period. However, since the bending and springback are synchronous, the simulation diagram of tube deformation shape at  $t = 2.1$  s and 2.11 s is selected for comparison, as shown in Fig. 14. It can be seen from the figure that the bending angle of the tube at  $t = 2.11$  s is slightly less than that at the time of  $t = 2.1$  s, and the bending of the tube in this short time is ignored. Therefore, it can be judged that the tube springback occurs in this short time, and the stress release process is accompanied by springback.

As shown in Table 2, with the same A-value and the same position, the stress release value of the outer side is higher than that of the inner side, indicating that the outer springback is higher than the inner side A-value and the same position. At the same A and different positions, the inner and outer stress release laws are satisfied:  $L1 < L3 < L2$ . The same is true for the inner and outer springback.

**3.5 Comparison of springback between T2 copper and AA6061 tubes**

The following model can be obtained by analyzing Eq. (13) and Eq. (14) that under the same bending angle,

**Fig. 14** Comparison of bending angles of Al tube at different times. **a**  $t = 2.1$  s; **b** 2.11 s

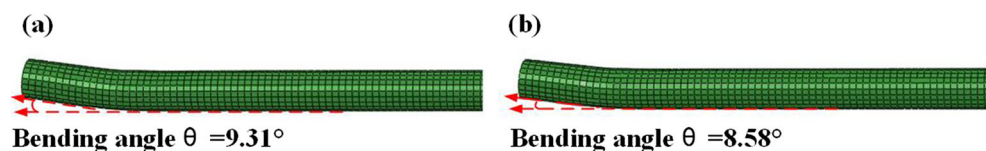
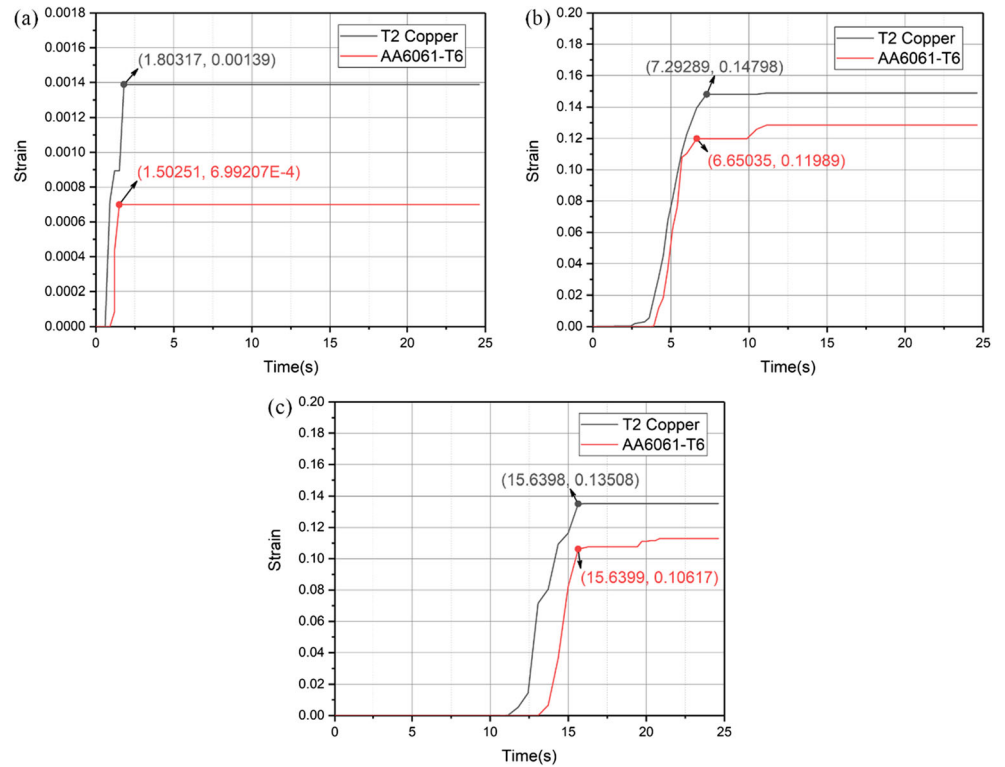


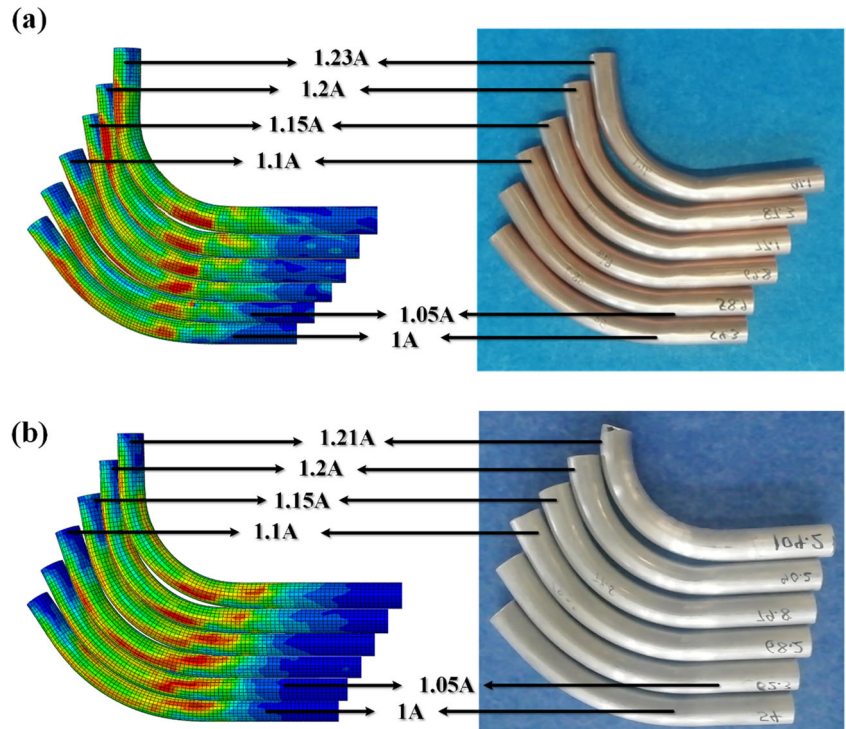
**Fig. 15** Comparison of strain in different bending sections of T2-Cu and AA6061-T6 tubes. **a** Inter side of L1. **b** Inter side of L2. **c** Inter side of L3



the higher the strain change value of tubes during the bending process, the higher the A, B values, and the springback angle. The reason for making the springback angle of T2-Cu tubes larger than AA6061-T6 tubes was

explained by extracting the strain-time curves of simulation results of the AA6061-T6 tube bending process with “1.2A,” and that of T2 copper tube with “1.23A” as depicted in Fig. 15. The extracted points are the

**Fig. 16** Comparison of experimental and simulated results. **a** T2 copper tubes; **b** Al60661-T6 tubes



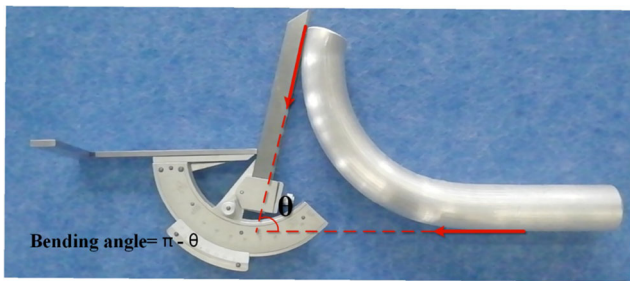


Fig. 17 Measurement of bending angle

inner side midpoint of the three sections of the bending process described in Fig. 8. Under the premise of the same bending angle, the value of strain change in each section of the bending process shows that springback of T2-Cu tubes is higher than that of AA6061-T6 tubes as depicted in Fig. 8.

### 4 Free bending experiment

The free bending experiments of T2-Cu and AA6061-T6 tubes were accomplished based on the FE simulation results. The results of different experiments under different A-values for T2-Cu and AA6061-T6 tubes are depicted in Fig. 16. Figure 17 describes the measurement of bending angles, and the bending radius of various bending components was measured by an indirect method introduced in Fig. 17. The Y-axis feed value regarded as the arc length of bending components was read from Fig. 18a and b. The ratio of the arc length to the bending angle is the bending radius. After calculation by the above method, the comparison for the bending radius and bending angles between the experimental and the simulation results is listed in Tables 3 and 4. The difference between the above two under each condition is less than 5%, proving that the experimental value is reliable.

Table 3 Comparison of the bending angles between the experimental results and the simulation results

| Experimental materials |       | Simulation value (°) | Experimental value (°) | Difference value (%) |
|------------------------|-------|----------------------|------------------------|----------------------|
| T2 copper tubes        | 1A    | 54.0                 | 54.3                   | 0.56                 |
|                        | 1.05A | 60.4                 | 58.9                   | -2.48                |
|                        | 1.1A  | 69.0                 | 69.8                   | 1.16                 |
|                        | 1.15A | 76.0                 | 77.1                   | 1.45                 |
|                        | 1.2A  | 85.6                 | 87.3                   | 1.99                 |
|                        | 1.23A | 90.0                 | 91.1                   | 1.22                 |
| Al6061-T6 tubes        | 1A    | 56.7                 | 54.0                   | -1.89                |
|                        | 1.05A | 63.5                 | 62.3                   | -1.20                |
|                        | 1.1A  | 71.5                 | 68.2                   | -4.62                |
|                        | 1.15A | 79.8                 | 79.8                   | 0.00                 |
|                        | 1.2A  | 88.4                 | 90.2                   | 2.04                 |
|                        | 1.21A | 90.0                 | 93.0                   | 3.33                 |

Analyzing data from Tables 3 and 4, the laws that the springback of tubes increases with A-value in the 3D bending process and springback of T2 copper tubes are more significant than AA6061-T6 tubes can still be drawn.

### 5 Conclusions

In this investigation, FE modeling and experiment were carried out using T2-Cu and AA6061-T6 tubes. It was realized that the two materials not only have different springback angles under various A-values but also have different springbacks at the three forming sections (L1, L2, and L3) of each material. Based on the results acquired from the current study, the main conclusions can be deduced as follows:

Fig. 18 The feed value of Y-axis. a Initial position of Y-axis. b Y-axis position after bending procedure completed

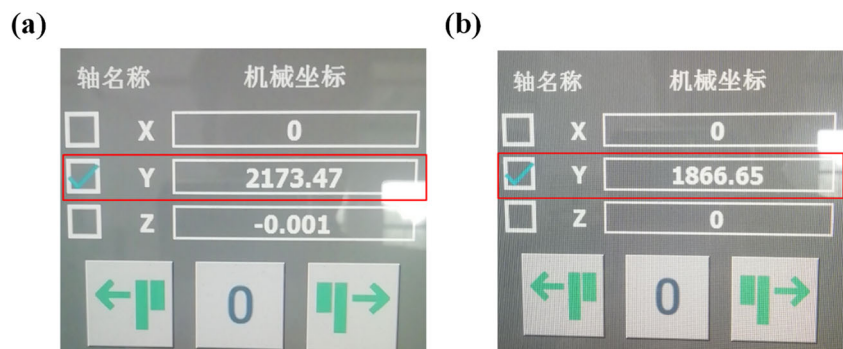


**Table 4** Comparison of the bending radius between the experimental results and the simulation results

| Experimental materials |       | Simulation value (°) | Experimental value (°) | Difference value (%) |
|------------------------|-------|----------------------|------------------------|----------------------|
| T2 copper tubes        | 1A    | 200.00               | 198.90                 | - 0.55               |
|                        | 1.05A | 178.80               | 183.36                 | 2.55                 |
|                        | 1.1A  | 156.52               | 154.73                 | - 1.15               |
|                        | 1.15A | 142.11               | 140.08                 | - 1.43               |
|                        | 1.2A  | 126.17               | 123.71                 | - 1.95               |
|                        | 1.23A | 120.00               | 118.55                 | - 1.21               |
| Al6061-T6 tubes        | 1A    | 190.48               | 200.00                 | 5.00                 |
|                        | 1.05A | 170.08               | 173.36                 | 1.93                 |
|                        | 1.1A  | 151.05               | 158.36                 | 4.84                 |
|                        | 1.15A | 135.34               | 135.34                 | 0.00                 |
|                        | 1.2A  | 122.17               | 119.73                 | - 2.00               |
|                        | 1.21A | 120.00               | 116.13                 | - 3.23               |

- (1) The higher A-value leads to the higher bending angle, the smaller bending radius, and the larger springback angle of Al and Cu tubes. The increase of the bending angle indicates that there are more and more materials for the tube's elastic deformation.
- (2) Under the same condition, the springback of the Cu tube is larger than that of the Al tube. The amount of springback increases with the increment of strain. The strain increment of the Cu tube is larger than that of the Al tube. Therefore, the springback of the Cu tube is higher than that of the Al tube.
- (3) The two materials have different springbacks at the three forming sections. The bending springback of the tube is a stress release process: the greater the stress release value, the greater the springback. The stress release values of Cu tube and Al tube in L1, L2, and L3 forming sections all meet the following rules:  $L1 < L3 < L2$ , so the springback amount of Cu and Al tubes at segments L1, L2, and L3 also satisfy:  $L1 < L3 < L2$ .

**Authors' contributions** Author 1: Wei Wang

- Conceived and designed the study
- Collected the data
- Contributed data or analysis tools
- Performed the experiments
- Performed the analysis
- Revised the analysis
- Wrote the paper
- Proofed reading

## Author 2: Shenghan Hu

- Conceived and designed the study
- Collected the data
- Contributed data or analysis tools
- Performed the experiments
- Performed the analysis
- Revised the analysis

- Wrote the paper
  - Proofed reading
- Author 3: Ali Abd El-Aty
- Conceived and designed the study
  - Collected the data
  - Contributed data or analysis tools
  - Performed the experiments
  - Performed the analysis
  - Revised the analysis
  - Wrote the paper
  - Proofed reading
- Author 4: Cong Wu
- Conceived and designed the study
  - Collected the data
  - Contributed data or analysis tools
  - Performed the experiments
  - Performed the analysis
  - Revised the analysis
  - Wrote the paper
  - Proofed reading
- Author 5: Qiucheng Yang
- Conceived and designed the study
  - Collected the data
  - Contributed data or analysis tools
  - Performed the experiments
  - Performed the analysis
  - Revised the analysis
  - Wrote the paper
  - Proofed reading
- Author 6: Hao Chen
- Conceived and designed the study
  - Collected the data
  - Contributed data or analysis tools
  - Performed the experiments
  - Performed the analysis
  - Revised the analysis
  - Wrote the paper
  - Proofed reading
- Author 7: Yizhou Shen
- Conceived and designed the study
  - Collected the data
  - Contributed data or analysis tools
  - Performed the experiments
  - Performed the analysis
  - Revised the analysis
  - Wrote the paper
  - Proofed reading
- Author 8: Jie Tao
- Conceived and designed the study
  - Collected the data
  - Contributed data or analysis tools
  - Performed the experiments
  - Performed the analysis
  - Revised the analysis
  - Wrote the paper
  - Proofed reading

**Funding** This study was funded National Natural Science Foundation International (regional) cooperation and exchange project (Grant No. 51711540301), the National Natural Science Foundation of China (Grant No. 51875548), Natural Science Foundation of Jiangsu Province (Grant No. SBK2020044364), National Natural Science Foundation International (regional) cooperation and exchange project (Grant No.51711540301), Jiangsu Province Key Research and Development Project (No. BE2019007-2), Opening Project of Jiangsu Key

Laboratory of Advanced Structural Materials and Application Technology (No. ASMA201903), National Natural Science Foundation of China (No. U1937206), and the Fundamental Research Funds for the Central Universities (No. NT2020015).

**Data availability** The data that support the findings of this study are available on request from the corresponding author.

### Compliance with ethical standards

**Ethical approval** For this type of study, ethics approval was not required.

**Consent to participate** For this type of study, consent to participate was not required.

**Consent to publish** For this type of study, consent to publish was not required.

**Competing interests** The authors declare that they have no competing interests.

### References

- Guo XZ, Ma YN, Chen WL, Xiong H, Xu Y, El-Aty AA, Jin K (2018) Simulation and experimental research of the free bending process of a spatial tube[J]. *J Mater Process Technol* 255:137–149
- Cheng X, Guo XZ, Tao J, Xu Y, El-Aty AA, Liu H (2019) Investigation of the effect of relative thickness ( $t_0/d_0$ ) on the formability of the AA6061 tubes during free bending process[J]. *Int J Mech Sci* 160:103–113
- Li T, Wang H, El-Aty AA, Li J, Zhang Y, Wei WB, Chen H, Cheng X, Tao J, Guo XZ (2020) Theoretical modelling and finite element simulation of AA6061 involute components based on 3D free bending process[J]. *Int J Mech Sci* 178:105607
- Shahabia M, Nayebe A (2015) Springback FE modeling of titanium alloy tubes bending using various hardening models[J]. *Struct Eng Mech* 56(3):369–383
- Li H, Shi KP, Yang H, Tian YL (2012) Springback law of thin-walled 6061-T4 Al-alloy tube upon bending[J]. *Trans Nonferrous Metals Soc China* 22:s357–s363
- Daxin E, Liu YF (2010) Springback and time-dependent springback of 1Cr18Ni9Ti stainless steel tubes under bending[J]. *Mater Des* 31(3):1256–1261
- Zhan M, Yang H, Huang L, Gu RJ (2006) Spring-back analysis of numerical control bending of thin-walled tube using numerical-analytic method[J]. *J Mater Process Technol* 177(1-3):197–201
- Cai W, Shuang YH, Gou YJ, Mao FL (2018) Research on springback of coreless bending of 0cr18ni9 pipe with large curvature[J]. *J Plast Eng* 25(06):70–76
- Zhu YX, Chen W, Li HP, Liu YL, Chen L (2018) Springback study of rectangular H96 tube[J]. *Int. J Mech Sci* 138-139:282–294
- Liao J, Xue X, Barlat F, Gracio J (2014) Material modelling and springback analysis for multi-stage rotary draw bending of thin-walled tube using homogeneous anisotropic hardening model[J]. *Procedia Eng* 81:1228–1233
- Wang GX, Yang H, Li H, Zhan M, Gu RJ (2005) Experimental study of the influence of processing parameters on forming quality of thin-walled NC bending tube[J]. *J Mater Process Technol* 24(8):995–998
- Zhai RX, Ding XH, Yu SM, Wang CG (2018) Stretch bending and springback of profile in the loading method of prebending and tension[J]. *Int J Mech Sci* 144:746–764
- Wu JJ, Zhang ZK, Shang Q, Li FF, Wang YA, Hui Y, Fan H (2017) A method for investigating the springback behavior of 3D tubes[J]. *Int J Mech Sci* 131-132:191–204
- Zhou YP, Li PF, Li MZ, Wang LY, Sun S (2018) Residual stress and springback analysis for 304 stainless steel tubes in flexible-bending process[J]. *Int J Adv Manuf Technol* 94(1-4):1317–1325
- Ahn K, Lee K-H, Lee J-S, Won C, Yoon J (2020) Analytic springback prediction in cylindrical tube bending for helical tube steam generator[J]. *Nucl Eng Technol* 52(9):2100–2106
- Gu RJ, Yang H, Zhan M, Li H (2006) Springback of thin-walled tube NC precision bending and its numerical simulation[J]. *Trans Nonferrous Metals Soc China* S2:631–638
- Li Y, Li A, Yue Z, Qiu L, Badreddine H, Gao J, Wang Y (2020) Springback prediction of AL6061 pipe in free bending process based on finite element and analytic methods[J]. *Int J Adv Manuf Tech* 109(7-8):1789–1799
- Guo XZ, Wei WB, Xu Y, El-Aty AA, Liu H, Wang H, Luo XY, Tao J (2019) Wall thickness distribution of Cu-Al bimetallic tube based on free bending process[J]. *Int J Mech Sci* 150:12–19
- Guo XZ, Cheng X, Xu Y, Tao J, El-Aty AA, Liu H (2020) Finite element modelling and experimental investigation of the impact of filling different materials in copper tubes during 3D free bending process[J]. *Chin J Aeronaut* 33(2):721–729
- Fang J (2015) 21-6-9 numerical control bending forming law of high strength stainless steel tube[D]. Nanjing university of aeronautics and astronautics, Nanjing
- Zhang S, Wu JJ, Deng LC et al (2014) Prediction of curvature bending rebound of small diameter thick wall tubes[J]. *Mater Sci Technol* 22(3):1–6
- Guo XZ, Xiong H, Li H, Xu Y, Ma ZQ, El-Aty AA, Ma YN, Jin K (2018) Forming characteristics of tube free-bending with small bending radii based on a new spherical connection[J]. *Int J Mach Tools Manuf* 133:72–84
- Gantner P, Harrison DK, De Silva AKM, Bauer H (2007) The development of a simulation model and the determination of the die control data for the free-bending technique[J]. *SAGE Publications* 221(2):163–171
- Zhan M, Wang Y, Yang H, Long H (2016) An analytic model for tube bending springback considering different parameter variations of Ti-alloy tubes[J]. *J Mater Process Technol* 236:123–137

**Publisher's note** Springer Nature remains neutral with regard to jurisdictional claims in published maps and institutional affiliations.